Tests at the MMT of Multi-Laser Guide Star Wavefront Sensing for Advanced Adaptive Optics

M. Lloyd-Hart, C. Baranec, N. M. Milton, T. Stalcup, M. Snyder, N. Putnam, and J. R. P. Angel

Steward Observatory, The University of Arizona, Tucson, AZ 85721

mhart@as.arizona.edu

Key advances in adaptive optics (AO) for both astronomical and military applications will be enabled through the deployment of multiple laser guide stars on a single telescope. Wider compensated fields of view than are now seen with conventional AO systems, even those equipped with single laser beacons, will be achieved, with less field dependence of the delivered point-spread function. Correction to the diffraction limit over 2 arcminute fields with multi-conjugate AO, and partial correction over 10 arcminutes with ground-layer AO is anticipated.

We describe the first multi-laser wavefront sensing system designed to support these modes of AO, now operating at the 6.5 m MMT in Arizona. Five beacons are made by Rayleigh scattering of laser beams at 532 nm integrated over a range from 20 to 29 km by dynamic refocus of the telescope optics. The return light is analyzed by a unique Shack-Hartmann sensor that places all five beacons on a single detector, with electronic shuttering to implement the beacon range gate. Data comprise simultaneous measurements of wavefronts sensed by the beacons and a series of natural stars. We find the average beacon wavefront gives a good measurement of ground layer aberration. With the new data, we are investigating tomographic wavefront sensing: three-dimensional reconstruction of the atmospheric aberration, a prerequisite for wide-field diffraction-limited imaging. We describe the application of these new modes of AO operation to high-resolution satellite imaging, and our plans for an early demonstration at the MMT of closed-loop AO in ground layer and tomographic correction modes.

1. Introduction

Ground based astronomical telescopes with adaptive correction are able to exceed the resolution of the Hubble Space Telescope. However, their use is currently limited almost exclusively to a small fraction of the sky, in small fields of view around the stars required to measure the wavefront error. These stars must be relatively bright because removal of atmospheric blurring requires rapidly updated command signals to the wavefront corrector. The radius of the compensated field around the star, the isoplanatic angle, is limited because atmospheric turbulence extends many kilometers above the ground, so the integrated wavefront distortion depends sensitively on the direction of view.

For telescopes in the current 8–10 m class, the limitation on brightness, though not on corrected field of view, can be largely removed by use of a laser beam projected toward a faint astronomical target to create an artificial beacon. Light from a sodium resonance beacon generated at $\sim$ 90 km altitude follows the path

taken by light from the target closely enough that a good estimate of the aberrations in the latter can be derived. The laser light, however, does not come from infinity, and as the telescope diameter is increased, the mismatch in optical paths (the cone effect) eventually becomes so severe that no useful recovery of stellar wavefronts can be made.

Extremely large telescopes (ELTs) with diameters greater than 25 m will therefore require a further advance to recover diffraction-limited imaging with AO. Multiple beacons placed so that their light collectively samples the full volume of atmosphere traversed by light from a target can in principle provide the solution. The instantaneous stellar wavefront would be computed by a tomographic algorithm applied to the wavefronts measured from all the beacons.[1–3] This method, implemented with sodium beacon lasers, is planned for the Giant Magellan Telescope (GMT),[4] and for the Thirty Meter Telescope,[5] to recover the full resolution of their apertures.

In the simplest application of tomography, the stellar wavefront along a single line of sight is estimated from all the measured beacon wavefronts, and the compensating phase is applied to a single deformable mirror (DM). The technique, called Laser Tomography AO (LTAO), delivers a diffraction-limited field of view limited by the normal isoplanatic angle.

Once a telescope is equipped with multiple laser beacons and tomographic analysis, a variety of altitude-conjugated AO techniques are enabled: diffraction-limited resolution over a field many times the isoplanatic angle with multi-conjugate and multi-object AO (MCAO, MOAO),[5–8] and partially improved seeing over a yet larger field with ground-layer AO (GLAO).

Of these advanced techniques, only MCAO has yet been attempted, in experiments at two solar telescopes.[9,10] Numerical models of GLAO based on measurements of the vertical distribution of turbulence at a number of sites,[11–13] suggest the potential for dramatic image improvement in the near infrared.[14] have modeled GLAO performance in detail, using vertical distributions of turbulence seen at Cerro Pachòn that put roughly 2/3 of the power in the ground layer. With a pentagonal arrangement of LGS and an adaptive secondary mirror, the study concluded that the median image width in K band would improve from 0.42 to 0.18 arcsec for a 5 arcmin field and to 0.25 arcsec over 10 arcmin.

Ground-breaking work by Ragazzoni et al.[15] has hinted at the power of tomographic wavefront sensing. That paper describes the first experiments in tomography, at the Telescopio Nazionale Galileo, in which wavefront estimates were obtained simultaneously from a close asterism of four natural stars through the simple expedient of defocusing the telescope. The instantaneous Zernike modal amplitudes measured from one star were compared to estimates derived from the modal amplitudes of the other three. Tomographic estimation from the three beacon stars was shown to be substantially superior to a simple average, or the use of any one of the three individually.

We report in this paper results from the first implementation of a wavefront sensing system based on a constellation of multiple laser beacons. Previous work on laser-guided AO has been confined to a single beacon, usually created by resonance scattering in the sodium layer at 90 km altitude.[16–18] For our work at the 6.5 m MMT we have created five beacons, generated by Rayleigh scattering. Commercial, pulsed doubled-YAG lasers at 532 nm are used, readily available at moderate cost. Single Rayleigh beacons gated to an altitude of $\sim$ 12 km have previously been used for AO with small telescopes[19] but the strong focus anisoplanatism and incomplete sampling of higher turbulence make a single such beacon of little value for an 8 m class telescope.

For our experiments, though, Rayleigh beacons are ideal. In our system the range gate is centered at 24 km altitude, high enough to sample collectively most of the turbulence. To increase signal strength, the sensor

system includes optics to focus the telescope dynamically, to maintain sharp images of each laser pulse at it rises from 20 to 29 km.[20,21] In this way, the range gate is extended to be $\sim 20\times$ longer than the telescope's normal depth of field. Even at this high altitude, focus anisoplanatism would remain a difficulty with a single beacon, but with five, it is not an issue, precisely because our goal is the development of tomographic techniques. The practical advantage is that the current high capital and operating costs of tuned sodium lasers for resonance scattering are avoided, allowing us to make an early start.

2. Instrument description

The multi-beacon experiment at the MMT has been designed to investigate both full tomographic wavefront sensing needed for diffraction limited imaging and ground layer sensing to improve the seeing. With these goals in mind, and guided by previous modeling of tomography,[22] we have built a pentagonal constellation of Rayleigh laser guide stars (RLGS) with a diameter of 2 arcmin. This field is not as large as one would choose for ground-layer sensing alone, given theoretical predictions of the size of the field that might be corrected by a GLAO system; nevertheless, it is capable of taking the first steps to quantifying the degree of correction to be expected of a closed-loop system.

The experimental set-up divides in two parts: the lasers and beam projector optics to generate the five RLGS, and the wavefront sensor detectors and associated optics mounted at the telescope's Cassegrain focus.

2.1. Generating the laser guide stars

The mean range chosen for the Rayleigh return is 24 km, where the beacons form a pentagon 14 m in diameter. The collective volume filling of this arrangement allows for three-dimensional sensing of the turbulence by tomography for ranges up to 10 km, and thus avoid the focal anisoplanatism that would arise from a single RLGS.

The projection system employs two frequency-doubled YAG lasers from Lightwave Electronics, rated at a nominal 15 W output each, operating at 532 nm and 5 kHz pulse repetition rate.[21] The two linearly polarized beams are combined with a polarizing beam splitter to produce a single, diffraction-limited beam measured at $\sim$ 27 W. In operation, synchronized pulses of light from the lasers are split by a computer-generated hologram in the projection optics to create the 5 beacons on a 2 arcmin diameter ring on the sky. The lasers and combining optics are attached directly to the 6.5 m telescope tube, with the power supplies and chiller in an adjacent room in the co-rotating MMT building. The laser heads are in a thermally controlled enclosure. At the top of the telescope tube on one side is a steering mirror close to an image of the exit pupil, used to compensate for slow misalignments in the projected beam direction caused by flexure and temperature changes. The hologram is also at this pupil. The beams are launched together through a single 50 cm diameter telephoto objective lens mounted centrally on the 6.5 m telescope axis, directly above the secondary mirror.

2.2. Cassegrain instrument for wavefront sensing

The wavefront sensor package mounts at the MMT's Cassegrain focus, and includes distinct optical arms for the RLGS and a natural star. The first comprises a novel sensor, which includes the dynamic focus optics, described in detail in,[20] and a single electronically shuttered CCD which images all five beacons.

We aim to measure laser returns from $\sim$ 24 km altitude, twice the height of earlier Rayleigh beacons,[19] to allow better sampling of high turbulent layers. Because the air at that altitude is only 10% of the sea-level density, we have developed a new technology to focus the telescope continuously to follow the rising pulse

from a Q-switched laser.[23,24] The sensitivity is thereby increased by an order of magnitude compared to conventional range gating methods. The dynamic focus of all five beacons is achieved by sinusoidal motion of a single 25 mm mirror placed at an image of the telescope pupil, with approximately one third of each cycle matched to the motion of the returning laser pulse.

The dynamic focus optics and mechanical resonator that moves the mirror are included in the fore-optics of the RLGS sensor. The resonator serves also as the system's master clock, triggering the laser pulses and the RLGS wavefront sensor (WFS) detector shutter at prescribed phase delays. In this way, each laser pulse is tracked in focus over a range gate from 20 to 29 km.

The refocused laser light is imaged onto a common 35 mm pupil, where a prism array[25] divides the light into 36 subapertures of equal size in a hexapolar geometry. A compound lens following the prism array images the beacons into five separate 36-spot Shack-Hartmann patterns on the detector, a CCID18 from Lincoln Laboratory. This is a 128×128 pixel frame transfer device with 16 output amplifiers and an electronic shutter. The controller, supplied by SciMeasure, reads the detector at frame rates up to 915 Hz. Operation of the electronic shutter during transitions of the CCD clock signals introduces additional noise into the image, so a carefully interleaved sequence is required of the clocks for the frame transfer and read operations, and of the shutter, which is triggered by the dynamic focus oscillator.

In order to explore the effectiveness of the RLGS wavefront sensor as a function of position within the field, a second optical arm of the Cassegrain instrument was built with a standard Shack-Hartmann sensor to measure wavefronts from natural stars. A dichroic splitter covering a 3 arcmin field separates the beams to the two wavefront sensors, transmitting the laser light to the LGS arm and reflecting starlight at wavelengths longward of 650 nm to the star sensor.

The star WFS is a copy of the one normally used for adaptive optics with the MMT adaptive secondary mirror.[26] The pupil is divided into a 12×12 array of square subapertures of which 108 are illuminated. The camera uses an E2V CCD39 frame transfer detector with 80×80 pixels. The whole WFS and associated optics were placed on a mechanical slide, allowing translation in one axis across the 2 arcmin field covered by the beacons. In practice, the telescope is offset a prescribed angle from the nominal stellar coordinates, and the WFS is moved by a corresponding angle in order to reacquire the star.

In operation, both sensors are run simultaneously, but asynchronously, with the latter providing measurements of the true stellar wavefront aberration to which reconstructions derived from the recorded RLGS signals can be compared. The star WFS was typically run at its maximum unbinned frame rate of 108 frames per second, with the RLGS sensor running at approximately half that frame rate. Data capture was externally registered in time by the use of synchronized flashing LEDs placed in front and to the side of each camera, running at approximately 1 Hz.

3. Observations and analysis

3.1. Photometric and imaging performance of the RLGS wavefront sensor

We have quantified the return flux from the RLGS using observations of the spectrophotometric standard star HD192281 made through a filter of 3 nm equivalent width, centered on 532 nm. To do so, the prism array defining the subapertures in the RLGS WFS was replaced with a flat optic of the same construction, and the telescope refocused to account for the substantial difference in stellar and beacon conjugates. The detected quantum efficiency of the WFS, including the telescope, optics and detector, was found to be 15%. Throughput of the beam projector optics was estimated at 73% from measurements of each element individually.

During observations of the RLGS, the detected return flux at zenith was 1.1×10^5 photoelectrons $\mathrm{m}^{-2}\mathrm{J}^{-1}$ over a range gate of 20–29 km. Accounting for our estimated efficiencies in both the outgoing and incoming beams, this amounts to 1.0×10^6 ph m^{-2} at the telescope aperture per joule at the output of the beam projector. The expected flux has been calculated from the lidar equation [27, p. 222], and the atmospheric transmission [28, p. 264], taking into account the atmospheric temperature and pressure profile measured by a routine meteorological balloon flight from nearby Tucson International Airport at approximately the same time as the observations. The agreement, within 2%, is good; fortuitously so, since the uncertainty in our estimate of the projected power is 10–20%, dominated by uncertainty in the calibration of the lasers' built-in power meters. The return flux is as bright as a star of $m_v = 9.9$ seen through a V filter, and is similar to the range of returns from sodium beacons:,[29] for instance, measured 1.2×10^6 ph $\mathrm{m}^{-2}\mathrm{J}^{-1}$.

An unusual problem with the CCD in the RLGS WFS prevented the formation of sharp images. The typical full width at half maximum (FWHM) of the Shack-Hartmann spots was found to be 4.4 pixels (equivalent to 3.7 arcsec) when images of the beacons recorded independently on a separate acquisition camera were measured to have a FWHM of ~ 1.5 arcsec. A replacement chip has since been installed that shows no sign of this blurring. The spot separation, set by the WFS optics, was just 4 arcsec, so that there was substantial overlap of neighbouring spot images. An iterative deconvolution algorithm was required to recover useable spot positions. Furthermore, the increase in width reduced the signal-to-noise (S/N) ratio of the determination of each spot's position by a factor of ~ 2.5. An examination of the power spectral densities of the reconstructed modal amplitudes from the RLGS showed that frequencies above 15 Hz were dominated by noise rather than atmospheric signal. In the following analysis, therefore, a low-pass filter with a sharp cut at 15 Hz was applied to the data.

3.2. Comparison of laser and natural star wavefronts

Wavefront data were recorded during a 2 hr period on 2004 September 30, during which the seeing, 1.0 arcsec in V band, was worse than median for the telescope. The recorded data are frames from the RLGS and star WFS cameras, in near-continuous sequences of 9 s. Figure 1 shows sample frames taken simultaneously from the two cameras, and the corresponding reconstructed wavefronts, which in the case of the RLGS is the average of the five individual reconstructions. Both reconstructions are complete for the 25 modes in Zernike radial orders 2 through 6, although the resolution of the star wavefront sensor would allow more modal amplitudes to be calculated. Overall tip and tilt are of course not recovered from the lasers because of unknown beam motion in the upward paths.

Reconstructions of three individual modes as they evolve in time over a period of 3 s are shown, by way of example, in Figure 2. Values for the modal amplitudes for the average of the five beacons and the simultaneous values from a star near the center of the RLGS field are plotted. The generally good agreement indicates the presence of a strong ground layer. Aberration very close to the telescope's aperture will be common to all five RLGS and the star, and so will contribute in the same way to the variation of the modes. On the other hand, high-altitude turbulence will be sampled differently by the six light beams, and leads to the differences in the recovered amplitudes.

By subtracting the average RLGS wavefront from the stellar wavefront, one can obtain a quantitative estimate of the degree of correction possible with a simple ground-layer correcting scheme in which a DM conjugate to the telescope pupil is driven in response to the averaged beacon signals. Figure 3 shows the result for a 3 s sample of data. In general, we find that both the mean and the variance of the aberration are substantially reduced. We have investigated the potential for such correction for stars at several locations

across the RLGS field. The geometry of the beacons and the positions of the stars in the field used for this study is laid out in Figure 4.

For the five positions of the star, Table 1 shows the measured stellar wavefront aberration averaged over all the Zernike modes in each order, both before and after subtraction of the average RLGS wavefront. The value of r_0, deduced from the image motion of the Shack-Hartmann spots in the stellar WFS, and scaled to 500 nm wavelength, is also shown. The overall degree of correction varies from 40% near the center to 33% just outside the field covered by the RLGS.

Because the seeing varied significantly over the 2 hr period spanned by these observations, a direct comparison of wavefront correlation versus field angle is possible only by scaling the results to a common value. Figure 5 shows the results graphically, where the rms wavefront values in Table 1 have been scaled by a factor $(r_0/10.1\text{ cm})^{5/6}$, to the average value of r_0 of 10.1 cm seen during the observations. The greatest improvement is seen in the lowest orders, which is to be expected, both because the amplitudes of the lower order modes have larger variance and are therefore sensed with greater S/N ratio, and because their angular correlation scale is larger and therefore correction extends to higher altitude than for modes with high spatial frequency. We note also that random noise in the reconstructions will preferentially appear as differences amongst the five RLGS signals, and so our estimate of the correlation between the natural star and mean LGS wavefronts is conservative.

3.3. Vertical distribution of turbulence

In a simplified model in which the vertical distribution of turbulence is characterized by just two regimes, one near the ground that is well corrected, and the other at high altitude that is not corrected, one can readily calculate from our data the division of power in the aberration between the two. Under the assumption of a Kolmogorov spectrum, with an infinite outer scale, the mean square wavefront error in orders 2–6 is $0.118(D/r_0)^{5/3}$ rad^2 [27, p. 96]. A deficit of power is observed in the two tilt modes seen by the NGS WFS, which we attribute to a finite outer scale, but in second and higher orders, the effect is small. In these orders, the overall average ground-layer corrected residual error inside 70 arcsec radius is 464 nm, after the scaling to the mean seeing condition, yielding a value of r_0^{FA} for the uncorrected free atmosphere of 21.7 cm. The ground layer, then, is characterized by $r_0^{GL} = 12.3$ cm. This division of power of approximately 2/3 in the boundary layer and 1/3 in the free atmosphere is consistent with typical conditions at other sites.[30]

The thickness of the boundary layer is an important parameter which sets the corrected angular field of GLAO, and about which very little is known from current site surveys. Only recently have techniques been developed, such as SODAR[31] and SLODAR,[32] that address the detailed structure of the lowest levels of turbulence.

The turbulence-weighted mean height of the ground layer, h^{GL}, on the night of the observations can be estimated from the anisoplanatic behavior of the star and RLGS wavefronts. Figure 6 shows the mean square difference, as a function of angular separation, between the stellar wavefront and the simultaneous wavefront seen by four of the RLGS separately. One beacon, which gave wavefronts noticeably noisier than the other four, has been omitted. All 20 pairings of the five star positions and RLGS are plotted, after the same scaling to uniform r_0 as above. Also shown is a fitted curve of the form $y = a + b\ \theta^{5/3}$, the expected behavior of the anisoplanatic error. The fitted value of b is 42.5 ± 3.4 nm^2 arcsec$^{-5/3}$, where the uncertainty bounds an increase of 1 standard deviation in the χ^2 fit metric. This corresponds to an isoplanatic angle for the sensed boundary layer only of $\theta_0^{GL} = 20 \pm 1$ arcsec at 500 nm wavelength. The isoplanatic angle is related to h^{GL} through the standard formula $\theta_0 = 0.314 \cos\zeta\ r_0/h$ [27, p. 103], where ζ is the zenith angle. Taking the mean

value for these observations of $\cos\zeta = 0.95$, we find $h^{GL} = 380 \pm 15$ m for the boundary layer turbulence.

3.4. Projected GLAO gain with single and multiple RLGS

Under conditions of turbulence dominated by the ground layer, represented by our data, useful correction of seeing over a field of several arcminutes would be obtained with a simple correction system using just one Rayleigh beacon. By extrapolation of the curve of figure 6 we find that the rms aberration would be improved out to an angle, set by θ_0^{GL}, of $\sim$ 2.5 arcmin where the mean square residual caused by angular decorrelation of the ground layer equaled the contribution from the uncorrected free atmosphere. For such a simple correction system, the Rayleigh laser would be preferred over a sodium laser, because it weights the ground layer more strongly than the decorrelated higher layers. This is the approach adopted by the SOAR telescope.[33]

Wavefront correction with multiple beacons will perform better over wide fields. Averaging the beacon signals leads to higher rejection of free atmosphere aberration. Correction of stellar wavefronts in the direction of any given beacon will therefore be worse than if the signal from the beacon were used on its own. Over the field enclosed by the beacons, however, the wavefront compensation is expected to be more uniform. This effect, small but appreciable for the narrow constellation diameter we used, can be seen in the bottom trace in figure 6, where we superpose the residual error after correction with orders 2–6 from the multi-beacon average, from figure 5. The improvement at 1 arcmin radius is 13%.

4. Multi-beacon systems for current and future large telescopes

4.1. Practicality of multi-beacon systems

Implementation of practical AO systems with even one laser beacon has proven difficult. Sodium resonance systems were first proposed by,[34] yet are only now starting to be scientifically productive. As a result, the concepts required for ELTs, which must rely on still more complex systems with multiple beacons to realize their unique high resolution potential, have been even slower to develop.

Our first steps with a multi-beacon system give encouragement that the engineering difficulties can be overcome. The laser wavefront sensor system was designed to be as simple as possible, yet in its early stages, it has already proven capable of tracking the evolution of turbulence through 6th order Zernike modes over 6.5 m aperture. After the development of full tomographic reconstruction, correction to this degree in a closed loop implementation of LTAO would yield the diffraction limit at L band and longward, where the MMT is particularly powerful because of the low thermal background afforded by its adaptive secondary mirror.

A closed-loop system with broad scientific application will require response faster than the 15 Hz limit of the present data, and smaller subapertures to provide correction at shorter wavelengths. We plan to increase the resolution of our RLGS WFS to 60 subapertures, for correction reaching down to H band. Replacement of the CCD in that sensor to overcome the electronic blurring is expected to allow a substantial, though as yet unquantified, improvement. Photon noise does not set a practical limit; our measured flux at the WFS of 1.1×10^5 ph m^{-2}J^{-1} scales to 470 photons per subaperture per frame at the higher resolution, and a rate of 500 frames per second, adequate for full correction in K band. We envision also a further factor of 2.5 increase in photon flux by use of one 15 W laser for each beacon, which would allow operation through the H band. We note that the required beacon fluxes do not scale with aperture. Since the sodium beacons needed for ELTs yield about the same photon flux per watt, they need be no more powerful.

4.2. Multiple beacon concept for the Giant Magellan Telescope

The primary motivation for our work has been to understand the implementation of multi-beacon AO for the 25 m GMT.[35] Like the MMT, the GMT will be equipped with an adaptive secondary mirror, for large field GLAO correction and optimum performance in the thermal infrared. Of particular value has been the realization that LTAO and GLAO can be considered as the extremes of a continuum provided by beacon constellations of variable diameter. The minimum diameter is that necessary for the beams to probe the cylindrical volume traversed by light from a star on-axis, 1.5 arcmin for both the MMT with Rayleigh beacons and the GMT with sodium beacons. The maximum is $\sim$ 10 arcmin for wide field GLAO. In the multi-beacon implementation at the GMT a single set of 5 beacons and 5 wavefront sensors will be configured to cover this range of angles, in both the projection and sensing systems.

The GMT's AO system will incorporate features proven valuable in the MMT prototype. For example, the constellation of beacons will rotate about the telescope axis in order to counter field rotation. This is done at the MMT by turning the hologram that splits the single laser beam into five. At the GMT, where we anticipate a separate laser for each SLGS, the same task will instead be done with a K mirror. The sensing system will be fed by reflection from an 8 arcmin diameter dichroic mirror located above the direct Gregorian focus, and will incorporate a set of 5 articulated periscopes to feed light from the variable diameter constellation to fixed sensors. Such periscope optics are used now in the MMT, with a fixed reduction from 2 arcmin to 1 arcmin.

Perspective elongation of the WFS spots will be significant, $\sim$ 2.5 arcsec in the outer subapertures of the GMT. Among several solutions proposed,[36–39] our same dynamic refocus method at 5 kHz proven at the MMT could be used also with pulsed sodium lasers. The mechanical requirements for dynamic refocus on the larger telescope are not substantially more challenging than those already met at the MMT.[4]

4.3. RLGS constellations for 8 m class telescopes

The question arises as to whether a Rayleigh beacon constellation might be used as an alternative to a single or multiple sodium beacon for all AO operations at an 8 m telescope. While a single sodium beacon yields a good solution for the wavefront in the direction of the beam, the corrected field is small, limited by the usual angular anisoplanatism, and neither GLAO nor MCAO is possible. Multiple sodium beacons, the route being taken by the Gemini Observatory,[40] would add these capabilities, but at a high cost: the lasers are at present more than an order of magnitude more expensive than YAG lasers of the same power.

Implementations of tomography with RLGS have been studied in simulation.[24] modeled LTAO on an 8.4 m telescope with beacons range gated from 16–30 km. The corrected field of view remains small, but the axial K-band Strehl ratio was 0.55, comparable to performance predictions for 8 m telescopes with a single sodium beacon,[44] and the values now achieved in practice with a sodium beacon on the 3 m Shane telescope.[41] Although we have yet to simulate the comparison directly, we believe that it may be possible for LTAO with Rayleigh beacons to improve on the performance of a single sodium beacon. This is because the beacons can be arranged to provide 100% sampling of the atmosphere up to a height above almost all of the turbulence. This contrasts with the single sodium beacon case, where pupil coverage begins to drop immediately above the telescope, and falls off with height. A fraction of the turbulence is therefore unsensed, and more importantly, an unknown radial shear is introduced into the measured wavefront.

Figure 7 illustrates the fractional coverage of the area filled by on-axis starlight as a function of height by a single sodium beacon at 95 km range, and a regular pentagon of Rayleigh beacons in two cases. For the present constellation diameter of 2 arcmin and mean height of 24 km above a 6.5 m aperture, complete

coverage is available to 8 km. SCIDAR measurements above nearby Mt. Graham at the site of the Large Binocular Telescope[42] indicate that this is above typically 75% of the integrated C_n^2. Also shown is the case of a telescope of 8.0 m diameter, where the beacon diameter has been set to 86 arcsec, which gives the greatest height for full coverage, and the beacons projected to a mean range of 30 km. There, full coverage extends to 12 km. Even above that height, the Rayleigh beacons continue to provide better atmospheric sampling than the sodium up to 16.3 km, high enough to capture essentially 100% of the integrated C_n^2. Furthermore, tomographic reconstruction from the multiple Rayleigh beacons can in principle remove much of the focal anisoplanatism error inherent in the single sodium beacon measurement.

[22] have simulated the performance of MCAO on the MMT using two DMs and five Rayleigh beacons. They find that correction to the diffraction limit in the near IR is achieved over a 1 arcmin field, if the RLGS are each sampled at two distinct heights. Modeling by,[43] comparing MCAO systems on an 8 m telescope relying on Rayleigh beacons, sodium beacons, and a combination of the two, came to the same conclusion. That study shows further that the performance of the doubly-sampled Rayleigh system approaches that of sodium beacons in the same geometry. In practice, such a system of Rayleigh beacons could be built with polarized lasers and a Pockels cell to switch each returning beam from one WFS to another as each laser pulse rose through the atmosphere. The lasers, optics, and detectors to implement the scheme would be still much cheaper than the lasers needed to construct an equivalent with sodium lasers.

Rayleigh beacons at 30 km of similar brightness to those at 24 km at the MMT could be made with individual lasers of 15 W. The results of the models described above suggest that a system on an 8 m telescope that deployed five 15 W lasers, each dedicated to a single beacon, would allow the full range of LTAO, MCAO, and GLAO techniques to be implemented.

5. Conclusions

Our results show that a constellation of RLGS will be a powerful tool for ground-layer adaptive correction, when used to drive the MMT's adaptive secondary mirror. Other large telescopes equipped with adaptive secondaries and with similar boundary layers of $\sim$ 500 m mean thickness could also benefit with much improved K-band images expected from GLAO over a field as large as 10 arcmin diameter.

The main consideration that remains unexplored so far by our experiments is the power of tomographic methods applied to multiple Rayleigh beacons to recover higher layer aberrations as well as the ground layer. Open-loop field tests to show the practicality of tomography are planned with the MMT system. Wavefronts will be reconstructed as Zernike modes on two metapupils at the ground and at high altitude. The choice of the upper altitude is not critical.[1] The performance of LTAO will be evaluated by comparing direct measurements of natural star wavefronts in the center of the RLGS constellation with the integral of the tomographic solution along the same line of sight. In addition, the two-layer reconstructions will allow an early investigation of the performance of MCAO by exploring the agreement of the stellar and the integrated reconstructed wavefronts over the field enclosed by the RLGS.

Our plans also call for closed-loop demonstrations of both GLAO and LTAO with the MMT's adaptive secondary mirror, and the addition of a new real-time reconstructor computer recently received from Microgate S.r.l. Later, the addition of a second DM conjugated to high altitude will allow us to explore MCAO.

6. Acknowledgements

This work has been supported by the National Science Foundation under grant AST-0138347 and the Air Force Office of Scientific Research under grant F49620-01-1-0383. We are grateful for the continued support

of the MMT Observatory staff, particularly A. Milone, J. McAfee, and M. Alegria.

References

1. Lloyd-Hart, M., & Milton, N. M. 2003, JOSA A, 20, 1949
2. Ragazzoni, R., Marchetti, E., & Rigaut, F. 1999, A&A, 342, L53
3. Tokovinin, A. et al. 2001, A&A, 378, 710
4. Milton, N. M. et al. 2003, in Astronomical Adaptive Optics Systems and Applications, ed. R. K. Tyson & M. Lloyd-Hart (Proc. SPIE), 5169, 238
5. Dekany, R. G. et al. 2004, in Advancements in Adaptive Optics, ed. D. Bonaccini, B. L. Ellerbroek, & R. Ragazzoni (Proc. SPIE), 5490, 879
6. Beckers, J. M. 1988, in Very Large Telescopes and their Instrumentation, ed. M.-H. Ulrich, (Garching: ESO), 2, 693
7. Hammer, F. et al. 2002, in Scientific Drivers for ESO Future VLT/VLTI Instrumentation, ed. J. Bergeron & G. Monnet (Garching: ESO), 139
8. Tokovinin, A., Le Louarn, M., & Sarazin, M. 2000, JOSA A, 17, 1819
9. Berkefeld, T., Soltau, D., & von der Lühe, O. F. H. 2004, in Advancements in Adaptive Optics, ed. D. Bonaccini, B. L. Ellerbroek, & R. Ragazzoni (Proc. SPIE), 5490, 260
10. Langlois, M., Rimmele, T., & Moretto, G. 2004, in Telescopes and Instrumentation for Solar Astrophysics, ed. S. Fineschi & M. A. Gummin (Proc. SPIE), 5171, 187–194
11. Rigaut, F. 2002, in ESO Conf. Proc. 58, Beyond Conventional Adaptive Optics, ed. E. Vernet, R. Ragazzoni, S. Esposito, & N. Hubin (Garching: ESO), 11
12. Tokovinin, A. 2004, in Second Bäckaskog Workshop on Extremely Large Telescopes, ed. A. L. Ardeberg & T. Andersen (Proc. SPIE), 5382, 490
13. Tokovinin, A. 2004, PASP, 116, 941
14. Anderson, D. R. et al. 2005, PASP, in preparation
15. Ragazzoni, R., Marchetti, E., & Valente, G. 2000, Nature, 403, 54
16. Fugate, R. Q. 2003, in Large Ground-based Telescopes, ed. J. M. Oschmann & L. M. Stepp (Proc. SPIE) 4837, 934
17. Gavel, D. T. et al. 2000, in Adaptive Optical Systems Technology, ed. P. L. Wizinowich (Proc. SPIE), 4007, 63
18. Wizinowich, P. L. et al. 2004, in Advancements in Adaptive Optics, ed. D. Bonaccini, B. L. Ellerbroek, & R. Ragazzoni (Proc. SPIE) 5490, 1
19. Fugate, R. Q. et al. 1991, Nature, 353, 141
20. Georges, J. A. et al. 2003, in Adaptive Optical System Technologies II, ed. P. L. Wizinowich & D. Bonaccini (Proc. SPIE), 4839, 473
21. Stalcup, T. E. et al. 2004, in Advancements in Adaptive Optics, ed. D. Bonaccini, B. L. Ellerbroek, & R. Ragazzoni (Proc. SPIE), 5490, 1021
22. Lloyd-Hart, M., & Milton, N. M. 2002, in Adaptive Optical System Technologies II, ed. P. L. Wizinowich, D. Bonaccini (Proc. SPIE), 4839, 578
23. Angel, J. R. P., & Lloyd-Hart, M. 2000, in Adaptive Optical Systems Technology, ed. P. L. Wizinowich (Proc. SPIE), 4007, 270

24. Lloyd-Hart, M. et al. 2001, in Adaptive Optics Systems and Technology II, ed. R. K. Tyson, D. Bonaccini, & M. C. Roggemann (Proc. SPIE), 4494, 259
25. Putnam, N., Snyder, M., Stalcup, T., & Angel, R. 2004, in Advancements in Adaptive Optics, ed. D. Bonaccini, B. L. Ellerbroek, R. Ragazzoni (Proc. SPIE), 5490, 1138
26. Brusa, G. et al. 2004, in Advancements in Adaptive Optics, ed. D. Bonaccini, B. L. Ellerbroek, & R. Ragazzoni (Proc. SPIE), 5490, 23
27. Hardy, J. W. 1998, Adaptive Optics for Astronomical Telescopes, (New York: OUP)
28. Allen, C. W. 2000, Allen's Astrophysical Quantities, ed. A. N. Cox, (4th ed.; New York: Springer-Verlag)
29. Ge, J. et al. 1998, in Adaptive Optical System Technologies, ed. D. Bonaccini & R. K. Tyson (Proc. SPIE) 3353, 242
30. Verin, J. et al. 2000, "Gemini site testing campaign. Cerro Pachon and Cerro Tololo," Gemini RPT-AO-G0094, http://www.gemini.edu/
31. Skidmore, W. et al. 2004, in Ground-based Telescopes, ed. J. Oschmann (Proc. SPIE), 5489, 154
32. Wilson, R. W. 2002, MNRAS, 337, 103
33. Tokovinin, A. A. et al. 2004, in Adaptive Optical System Technologies II, ed. P. L. Wizinowich & D. Bonaccini (Proc. SPIE), 4839, 673
34. Happer, W., & MacDonald, G. J. 1983, MITRE Corp., MacLean, VA, JASON Report JSR-82-106
35. Johns, M. et al. 2004, in Ground-Based Telescopes, ed. J. M. Oschmann (Proc. SPIE), 5489, 441
36. Baranec, C., Bauman, B., & Lloyd-Hart, M. 2005, Opt. Lett., 30, 693
37. Beckers, J. M. 1992, Appl. Opt., 31, 6592
38. Beckers, J. M., Owner-Petersen, M., & Andersen, T. 2003 in Adaptive Optics Systems and Applications, ed. R. K. Tyson & M. Lloyd-Hart (Proc. SPIE), 5169, 123
39. Ribak, E. N., & Ragazzoni, R. 2004, Opt. Lett., 29, 1351
40. Ellerbroek, B. L. et al. 2003, in Adaptive Optical System Technologies II, ed. P. L. Wizinowich & D. Bonaccini (Proc. SPIE), 4839, 55
41. Gavel, D. et al. 2004 in Adaptive Optical System Technologies II, ed. P. L. Wizinowich & D. Bonaccini (Proc. SPIE), 4839, 354
42. McKenna, D. L. et al. 2003, in Adaptive Optical System Technologies II, ed. P. L. Wizinowich & D. Bonaccini (Proc. SPIE), 4839, 825
43. De la Rue, I. A., & Ellerbroek, B. L. 2001, in Adaptive Optics Systems and Technology II, ed. R. K. Tyson, D. Bonaccini, & M. C. Roggemann (Proc. SPIE), 4494, 290
44. Viard, E., Hubin, N., & Le Louarn, M. 2000, in Adaptive Opticsl Systems Technology, ed. P. L. Wizinowich (Proc. SPIE), 4007, 106

Table 1. Wavefront Aberration Before and After Correction

Zernike order	Set 1	Set 2	Set 3	Set 4	Set 5
2	462	572	513	571	559
	255	*316*	*308*	*349*	*343*
3	308	404	365	383	379
	198	*238*	*226*	*246*	*258*
4	223	285	261	276	269
	142	*181*	*168*	*184*	*190*
5	183	220	207	220	220
	140	*166*	*152*	*168*	*168*
6	159	184	175	194	170
	116	*143*	*130*	*154*	*143*
2–6	645	809	732	797	778
	397	*487*	*463*	*518*	*518*
r_0 (cm)	12.1	9.0	10.3	9.2	9.8

The root mean square stellar wavefront aberration in nm, averaged over the modes of each Zernike order, is shown before correction by the average RLGS signal (Roman), and after correction (below, italic). The sum over all measured orders is shown near the bottom, and the last line reports the observed value of r_0 in cm at 500 nm wavelength.

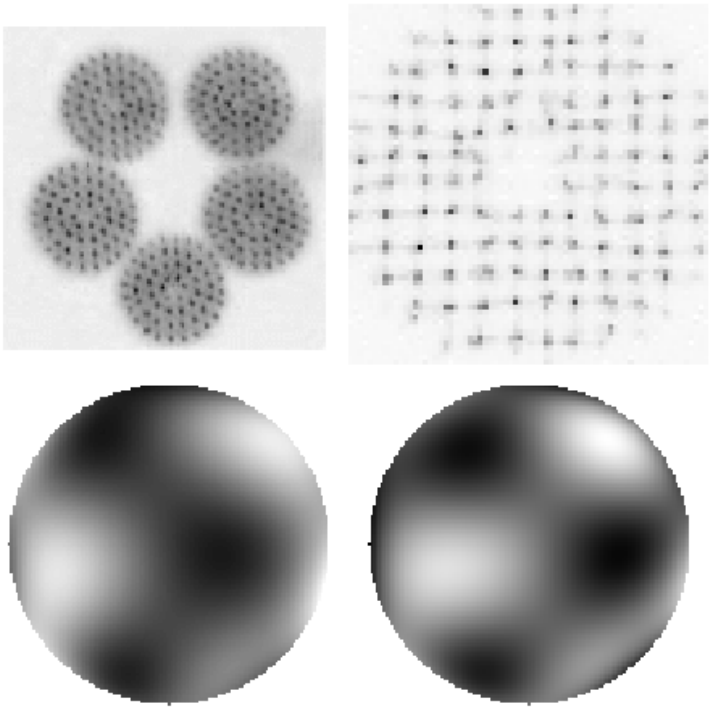

Fig. 1. Examples of the WFS data. The top panels show the WFS outputs, with the RLGS sensor on the left and the star WFS on the right. The bottom panels show the corresponding wavefronts reconstructed to Zernike order 6. The RLGS reconstruction is the average of the five individual wavefronts.

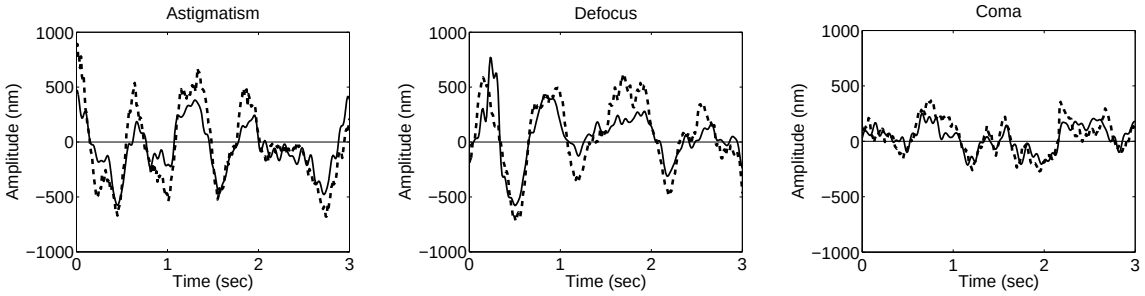

Fig. 2. Examples of the reconstruction of three Zernike modal amplitudes from the natural star (dashed line) and the average RLGS signal (solid line).

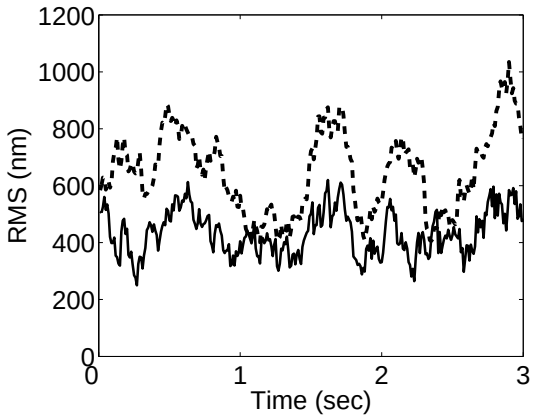

Fig. 3. Wavefront aberration averaged over the 6.5 m pupil for a representative sample of data. The dashed line shows the total for the reconstructed modes in Zernike orders 2 through 6 in the stellar wavefront. The solid line shows the residual after subtraction of the average RLGS wavefront.

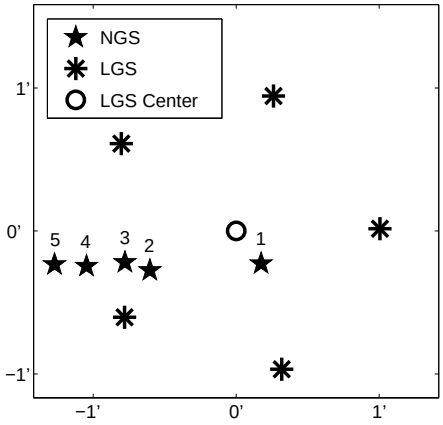

Fig. 4. Geometry on the sky of the RLGS used to measure the effect of boundary layer wavefront sensing. The labeled positions of the natural star where data were recorded are separated from the geometric center of the RLGS constellation by respectively 17.2, 39.8, 48.5, 64.5, and 77.5 arcsec.

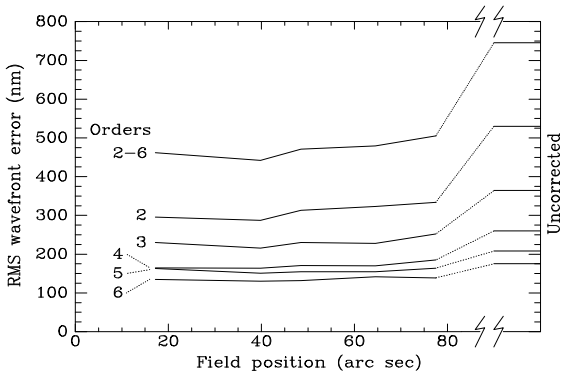

Fig. 5. Graph of the rms residual error in the stellar wavefront after subtraction of the average beacon wavefront measurement. The plotted lines show the residual in all the modes of Zernike radial orders 2 through 6, averaged over time, and the contributions of each order separately. The short lines on the right represent the uncorrected rms wavefront aberrations. The points at each field angle represent averages of 9 s of data, and in each case the data have been scaled to the mean r_0 seen during the observations of 10.1 cm at 500 nm wavelength.

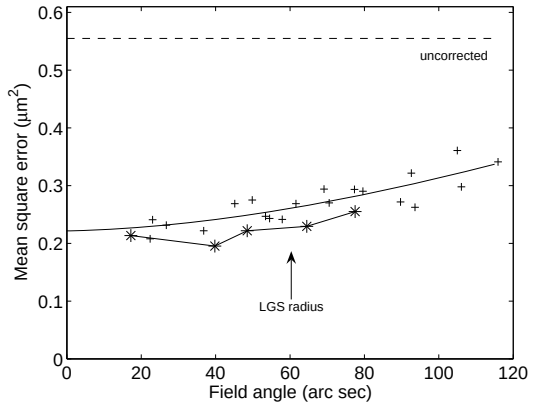

Fig. 6. The crosses show the mean square residual wavefront aberration after correction of the stellar wavefronts by simultaneous wavefronts from each of the RLGS, taken singly, as a function of the angular separation of the star and beacon. A fit to a 5/3 power law is shown as the solid curve. The stars reproduce the top line of figure 5, showing the correction obtained from the average of the beacon wavefronts from the same data. The dashed line shows the mean square aberration in the uncorrected stellar wavefronts.

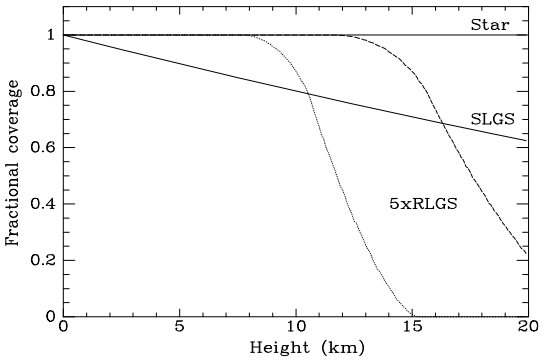

Fig. 7. Fractional intersection versus height of the area covered by light from an axial star and three LGS beacon arrangements: a single axial sodium laser guide star (SLGS) at 95 km range, and pentagonal constellations of Rayleigh laser guide stars (RLGS). We show the cases of a 6.5 m aperture, with the RLGS on a 60 arcsec radius at 24 km range (dotted line), and an 8.0 m aperture with RLGS at 43 arcsec radius and 30 km range (dashed line).